AIAA JOURNAL
Vol. 38, No. 7, July 2000

# Electrohydrodynamic Flow Control with a Glow-Discharge Surface Plasma

J. Reece Roth* and Daniel M. Sherman†
*University of Tennessee, Knoxville, Tennessee 37996*
and
Stephen P. Wilkinson‡
*NASA Langley Research Center, Hampton, Virginia 23681*

**Multiple flow diagnostics have been applied to planar panels covered by strips of glow-discharge surface plasma in atmospheric pressure air generated by the one atmosphere uniform glow discharge plasma. Direct drag measurements, smoke wire and titanium tetrachloride flow visualization, and boundary-layer velocity profiles were obtained. The plasma generated along streamwise-oriented, symmetric strip electrodes is shown to cause a large increase in drag, whereas the plasma along spanwise-oriented, asymmetric strip electrodes can generate a significant thrust. Flow visualization and mean velocity measurements show the primary cause of the phenomena to be a combination of mass transport and vortical structures induced by strong electrohydrodynamic body forces on the flow, known as paraelectric forcing.**

## Nomenclature

$C_d$ = drag coefficient
$d$ = electrode separation distance
$E$ = electric field
$F_b$ = body force
$f$, $F$ = frequency
$Gr$ = Grashof number [Eq. (5)]
$g$ = acceleration caused by gravity
$L$ = length scale for Grashof number
$p$ = pressure
$Re$ = unit Reynolds number, $m^{-1}$
$T$ = temperature
$U_\infty$ = freestream velocity
$u$ = velocity
$V$ = voltage
$x$ = streamwise coordinate
$y$ = vertical distance from wall
$\delta^*$ = boundary-layer velocity displacement thickness
$\varepsilon_0$ = permittivity of free space
$\nu$ = kinematic viscosity of air
$\rho_c$ = electrical charge density

## Introduction

ELECTROHYDRODYNAMIC (EHD) flow control relies upon the interaction between a partially ionized (or seeded) airflow and a strong electric field. This results in a Lorentzian collisional force on the neutral gas that may be useful in a variety of flow-control applications. For such a method to function in a gas so cool that Saha equilibrium (Ref. 1, pp. 135, 136) provides insufficient ionization, such as room temperature atmospheric air, an energy efficient source of charged particles is required. One method of efficiently securing an adequate number density of charged particles is to generate a weak plasma directly on the flow control surface. This approach can be implemented with a novel plasma source known as the one atmosphere uniform glow discharge plasma or OAUGDP.[2–4]

The OAUGDP is an efficient plasma generation technique that operates at atmospheric pressure. The gas between adjacent electrodes, at least one of which is covered with a thin dielectric, is ionized by a RF (radio frequency) voltage. The OAUGDP is not hard-starting and does not require external initiation (e.g., with a Tesla coil or spark gap). Under appropriate values of voltage, frequency, and electrode separation distance, a nonequilibrium, uniform glow discharge can be established. Typical excitation parameters are 1–20 kHz at several kilovolts, over a gap distance of a few millimeters. As a result of the very high collision rate between the relatively low density of charged particles and the background neutral gas at one atmosphere (several gigahertz for ions, several terahertz for electrons), bulk movement of the gas can be effected. Roth (Ref. 1, pp. 453–461) analyzes the OAUGDP from the perspective of a Lorentzian gas model and derives simple scaling expressions for the electrode spacing and electrical parameters. Massines et al.[5] report on an extensive, combined experimental and computational one-dimensional study of the OAUGDP in helium. They confirm that the OAUGDP is a true glow-discharge plasma and describe in detail the physical processes involved in its generation. Additional information on the OAUGDP is found in the patents cited in Refs. 2, 3, and 4.

Being a capacitive device, the OAUGDP utilizes displacement currents. The absence of large real currents in the OAUGDP protects its electrodes from erosion and reduces electrode heating. Its nature as a nonequilibrium, normal glow discharge allows it to operate at low areal power densities, consistent with the possibility of net energy savings in flight boundary-layer flow control or drag-reduction applications. For example, the OAUGDP can operate with a power of 0.3 $kW/m^2$ or less at one atmospheric pressure. For a long-range commercial transport at cruise conditions, the boundary-layer viscous dissipation value is estimated to be at least an order of magnitude higher.[6] Although there is no evidence or claim at this time that such a low OAUGDP power level can effectively control, say, a turbulent boundary flow at high-Reynolds-number flight conditions, there is clearly a sufficient energy margin available to justify investigation of a plasma-based flow-control technology.

This low-energy cost occurs for a fundamental reason. As shown in Ref. 5, the OAUGDP is a normal glow discharge that is created twice during each excitation cycle. As a normal glow discharge, the ionization process in the instantaneous cathode region occurs at the Stoletow point, which is about 81 eV per ion-electron pair for air (Ref. 1, pp. 246–251). This is, in principle, the lowest possible energy cost of producing an ion-electron pair in a plasma source.

Presented as Paper 98-0328 at the AIAA 36th Aerospace Sciences Meeting, Reno, NV, 12–15 January 1998; received 23 March 1999; revision received 28 October 1999; accepted for publication 28 October 1999. 

*Professor, Department of Electrical and Computer Engineering. Associate Fellow AIAA.
†Graduate Research Assistant, Plasma Sciences Laboratory.
‡Aerospace Engineer, Fluid Physics and Control Branch. Senior Member AIAA.

By comparison, the energy cost of producing ionization in other atmospheric plasma sources, such as plasma torches or arcjets, is about 10,000 eV/ion-electron pair.

The OAUGDP is a volumetric, glow-discharge plasma source that is fundamentally different from ion-wind flow-control concepts that rely on a corona discharge as an ion source. Malik et al.[7] used the ion-wind technique in a flat plate dc brush discharge fashion and were able to secure a small reduction in measured drag of about 5% for a turbulent boundary-layer flow at a length Reynolds number of approximately one million. Research was discontinued, however, because of the inability to scale the operation of the hardware to flight conditions. More recently, El-Khabiry and Colver[8] were able to produce up to 50% or more viscous drag reduction in very low-Reynolds-number flows (on the order of $10^5$). They used a corona discharge between spanwise wires on a flat surface for both dc and low-frequency (60 Hz) ac excitation. Again, the problem with this technique for flight applications is the inability to scale the corona-discharge effect to higher flow velocities. The OAUGDP, however, is more readily scaleable (Ref. 1, pp. 463–471) and, as will be shown, has the ability to function at airflow velocities up to at least 25 m/s.

## OAUGDP Mechanism and Paraelectric Forcing

The OAUGDP uses an ion-trapping principle that involves constrained, periodic oscillation of ions and electrons along electric filed lines between pairs of electrodes (Ref. 1, pp. 463–471). Based on straightforward Lorentzian electrodynamic analysis of the plasma, the ion-trapping mechanism identifies the pertinent independent variables as electric field strength, electrode separation distance, pressure, and RF electric field frequency. Roth (Ref. 1, pp. 463–471) gives a relation among these variables for a parallel plate geometry:

$$f \propto (E/pd) \tag{1}$$

A planar strip geometry will have a similar but more complicated relation because of its arched field lines, but the same qualitative functional dependencies would be expected to prevail. The electric field $E$ in Eq. (1) can be approximated by the electrode potential $V$ with $E = V/d$. This electric field must be at least 8.5 kV/cm to initiate a OAUGDP at 1 atm in air. Provided the operating parameters are in accordance with Eq. (1) the OAUGDP will function at 1 atm and produce a stable, steady-state glow discharge. A plasma-layer thickness of one or two millimeters was typical for the current experiments. Equation (1) does not represent a finely tuned phenomenon, and the parameters can vary over a useful range while maintaining the existence and uniformity of the plasma. If any of the parameters deviate sufficiently from Eq. (1), however, either the OAUGDP will cease to function, or its uniformity will degrade into a filamentary or dielectric barrier discharge.

A primary finding of the current research was observation of a paraelectric EHD body force caused by the OAUGD plasma. The paraelectric forcing effect is easily illustrated for the one-dimensional case by Poisson's equation (one of Maxwell's equations), which relates the local electric field gradient to the local charge density:

$$\frac{\mathrm{d}E}{\mathrm{d}x} = \frac{\rho_c}{\varepsilon_0} \tag{2}$$

By definition, the body force on a charged volume is given by

$$F_b = \rho_c E \tag{3}$$

Combining Eqs. (2) and (3) yields

$$F_b = \frac{\mathrm{d}}{\mathrm{d}x}\left(\frac{1}{2}\varepsilon_0 E^2\right) \tag{4}$$

Equation (4) shows that the magnitude and direction of the resultant body force is equal to the gradient of the local electric field energy density. For the current strip electrode models the electric field increases as one approaches the electrode edges. Using any self-consistent sign convention scheme, it can be shown that the body force is always directed toward the electrode, regardless of electrode polarity. For this reason the body force is referred to as *paraelectric*. In previous usage[9] paraelectric refers to the unidirectional force exerted on an electrically neutral dielectric body immersed in a non-uniform electric field. In the case of the OAUGDP, the physics is more involved because of the mobile charged particles. The mathematical relationship for the dielectric case, however, describing the force is similar to Eq. (4), and application of paraelectric terminology to the OAUGDP is appropriate.

## Experimental Apparatus

Both bench and low-speed wind-tunnel tests of various OAUGDP flat panel models were conducted. Typical implementation of the OAUGDP, as illustrated in Figs. 1a–1c, includes flush-mounted metallic strip electrodes on one side of a thin dielectric sheet with either similar strips or a uniform conducting plane on the other side. In Fig. 1a an array of electrode strips was situated on the top (flow) side of the board, and the bottom surface was a uniform conducting plane. The oscillating electric fields penetrate the dielectric, and the plasma forms near the edges of the electrodes above the upper surface. The configurations shown in Figs. 1b and 1c use strip electrodes on the lower surface enabling the plasma formation to be controlled by the relative placement of the upper and lower strips. Figures 1a and 1c are referred to as symmetric-planar and symmetric-staggered configurations, respectively, with equal regions of plasma forming along each upper electrode edge. Figure 1b is referred to as an asymmetric-staggered configuration, with the bulk of the plasma forming between the closest edges of the upper and lower strips. As will be shown, this is a requirement for generating a net force on the model using the paraelectric forcing effect.

The panels were constructed from a conventional printed circuit board material, which was woven-glass and epoxy, 0.75 mm thick, with double-sided, 1-oz (an industry standard designation) copper coating. The copper trace thickness was approximately 0.10 mm above the panel. For all models the upper surface electrodes were uncoated. Because the OAUGDP ion-trapping mechanism operates on displacement rather than real electrical currents, this surface can, if desired, be covered with a thin dielectric protective layer without qualitatively affecting the results reported herein. For wind-tunnel tests the panels were bonded to a 12.5-mm-thick fiberglass board that provided required stiffness and effectively suppressed plasma formation on the lower surfaces. For bench testing lower surface plasma was suppressed with vinyl adhesive tape. Table 1 presents the designations of the panels studied, their configuration in reference to Figs. 1a–1c, the upper electrode orientation in the wind tunnel, and pertinent dimensions. Figure 2 shows the detailed design for model C7-C that was typical of all wind-tunnel models.

The NASA Langley Research Center 7 × 11 Inch Low Speed Wind Tunnel (7 × 11) was used to measure direct drag and streamwise boundary-layer velocity profiles (determined from the pitot tube total pressure) on the models and to conduct smoke-wire flow

**Table 1 Panel designations and electrode dimensions**

| Panel designation | Corresponding sketch in Fig. 1 | Orientation with respect to freestream | Electrode width, mm | Electrode spacing,[a] mm |
|---|---|---|---|---|
| C7-A | 1a | Streamwise | 0.5 | 10.5 |
| C7-C | 1a | Spanwise | 0.5 | 10.5 |
| E6-C | 1b | Spanwise | 0.5 | 8.5 |

[a]Center-to-center spacing of electrodes.

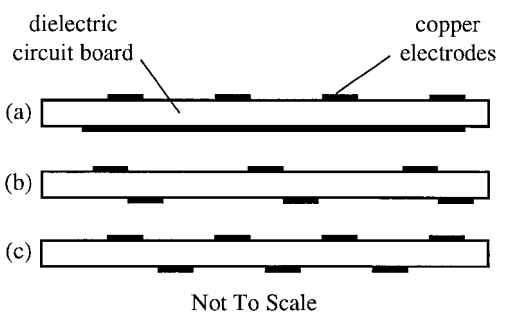


**Fig. 1 Plasma panel design concepts: a) symmetric planar, b) asymmetric staggered, and c) symmetric staggered.**

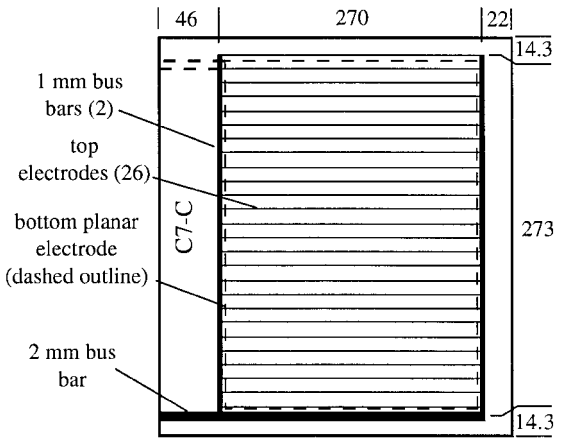


**Fig. 2 Dimensioned sketch of panel C7-C.**

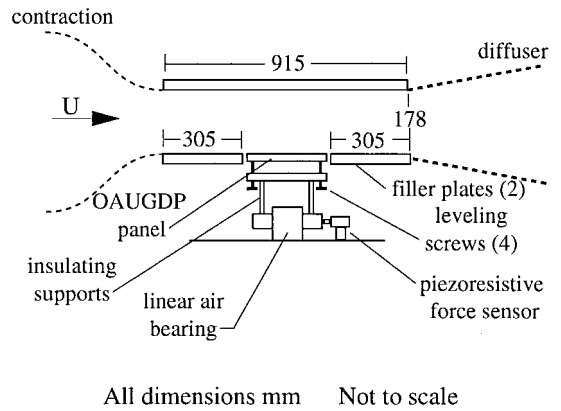


**Fig. 3 Cross-sectional sketch of Langley 7 × 11 Inch Low Speed Wind Tunnel test section.**

visualizations. The 7 × 11 is a closed return, unpressurized air facility with a test section having dimensions of 178 mm high × 279 mm wide × 914 mm long. The maximum freestream speed of the tunnel was approximately 26 m/s. For drag measurements a linear air-bearing drag balance was used with a piezoresistive force sensor. Flat-panel drag models were mounted on the drag balance in a 305 mm wide × 279 mm long central region of the lower test section wall. The test-section streamwise pressure gradient was nulled by a moveable side wall. The leakage flow in gaps surrounding the model was minimized by enclosing the test section in a pressure control box, the pressure in which was maintained equal to the freestream test section static pressure. Pitot pressure for boundary-layer velocity profiles measurements were made with a quartz electronic pressure transducer connected to a flattened hypodermic stainless-steel tube with end outer dimensions of 0.28 mm high × 0.65 mm wide and a 0.1-mm wall thickness. The probe was automatically traversed across the boundary layer by a commercial traverse mechanism. A sketch of the tunnel test section is presented in Fig. 3 showing the placement of the drag balance and other pertinent features.

The smoke-wire flow visualization in the 7 × 11 employed a 0.1-mm-diam stainless-steel wire coated with light mineral oil that formed small oil droplets along the wire. The wire was energized by a dc power supply, with requisite timing and control circuitry to operate a strobe light and a digital camera. Flow visualization photography for both the tunnel and bench testing was done with a digital, progressive-scan, monochromatic video camera with 768 by 484 pixel sensing elements and a f3.5–4.5, 75–200 mm zoom lens. The strobe light pulse had a width of approximately 50 $\mu$s. The bench apparatus used to photograph paraelectric flow acceleration effects in the absence of a mean flow consisted of a cubical, clear acrylic plastic box, approximately 45 cm on a side, used to shield the model from room air currents during photography. In this case incandescent lighting was used rather than the strobe. Further information concerning the wind-tunnel performance, instrumentation, and characteristics may be found in Refs. 6 and 10.

The power supply consisted of two 260 V rms, 1-kW variable frequency (up to 20 kHz) power amplifiers connected in series to a 10:1 step-up transformer. The parallel electrode strips on the top of a panel were bussed together and connected to one power supply terminal and the lower plane or array of electrodes underneath the panel to the other terminal. The parallel electrode strips on top of the panel were generally at the energizing voltage, whereas the lower electrode plane or strips was grounded. Configurations with the top surface electrodes grounded and the bottom plane or electrode strips at the excitation voltage would also produce plasma on the top surface and the effects reported here.

Impedance matching between the transformer secondary and plasma panel was not used for the current experiments as a matter of convenience and because it was not needed to see the paraelectric effects of interest in this study. Subsequent tests showed that impedance matching is desirable to promote an optimum uniform glow discharge. The lack of impedance matching, however, produced large reactive currents on the order of several hundred milliamps[6] that dumped unwanted charge onto the electrodes. Reference 5 shows that the residual electric charge remaining on the dielectric after each one-half excitation cycle is crucial to the formation of a truly uniform glow discharge. The unwanted charge deposit caused by the lack of impedance matching changes this voltage. This not only interferes with plasma formation and changes its duration, but also can lead to the formation of filamentary plasma instabilities. In addition to improving plasma uniformity, operation with a simple, passive impedance matching network can improve system efficiency and allow use of a lower-wattage power supply. Despite the lack of impedance matching and less than ideal glow uniformity, the paraelectric forcing mechanism just described remains operative. The results with a properly impedance matched system would be expected to be qualitatively similar to the current results.

## Flow Visualization

Figure 4 is a plan-view photograph of the model C7-C OAUGD plasma panel showing several adjacent energized electrodes. It was taken under low-room light level conditions with a conventional autoexposure 35-mm camera with a 75–200 mm f3.5–4.5 zoom lens and 400 ISO color slide film. This is a symmetric-planar electrode configuration (Fig. 1a), with equal electric field intensity to either side of the electrode strips. The light intensity of the glow discharge peaks slightly to either side of the electrodes, but extends with lower intensity over a much wider region. Because Fig. 4 is a time exposure over many cycles, the light represents both instantaneous anode and cathode processes. The dominant color of the glow is light blue.

Figures 5a and 5b are photographs illustrating the influence of paraelectric effects associated with the OAUGDP on a laminar jet of titanium tetrachloride vapor injected above a single, isolated, asymmetric-staggered electrode pair (i.e., Fig. 1b). The titanium tetrachloride reacts with humidity in atmospheric air to form an easily visible titanium dioxide stream. The test was conducted in the still air chamber, and the dominant direction of induced paraelectric flow along the wall was to the left. The lower electrode was staggered to the left of the upper electrode. The jet velocity at the tube exit is estimated to be no more than 1 m/s based on the laminar

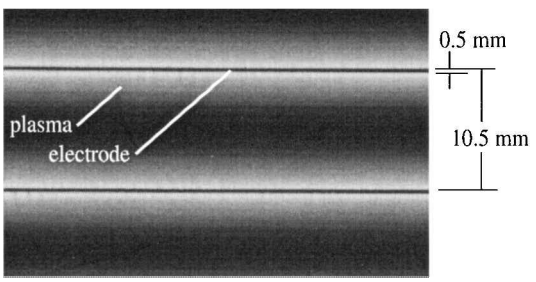


**Fig. 4 Photograph of plasma on panel C7-C.**

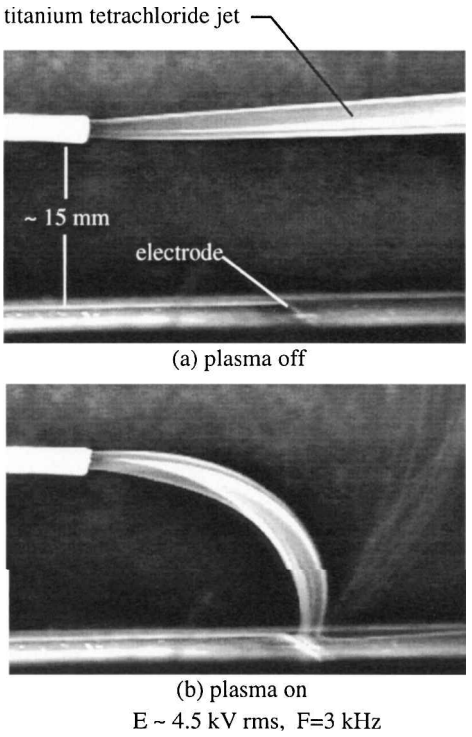


**Fig. 5 Demonstration of OAUGDP paraelectric force for single asymmetric-staggered electrode pair.**

appearance of the jet and assumption that the traditional pipe transition Reynolds number of $2 \times 10^3$ using air properties is valid for this case. The plasma is not visible in Fig. 5b because of the high level of illumination required to photographically capture the titanium dioxide stream. The downward deflection of the jet toward the electrode is caused by the paraelectric forcing effect within the plasma, Lorentzian momentum transfer from the ions to the neutral gas and to mass continuity. Strong attractive forces on the plasma ions in high electric field gradient regions near the electrode appear to pull the ionized flow toward the electrode. The forcing of the jet is not caused by charges induced on the titanium dioxide particles or other titanium tetrachloride reaction byproducts, which is evidenced by the fact that velocity profile and direct drag data (presented next) taken on other models in the absence of the flow marker particles are completely consistent with the flow visualization. This is also not a case of dielectrophoresis[9] because no smoke or air movement is observed until sufficient voltage is reached for the plasma to initiate, for the current models, approximately 1.5 kV rms.

Figures 6a and 6b are smoke-wire visualizations of model C7-A, a streamwise oriented, symmetric-planar configuration (Fig. 1a), in the wind tunnel with laminar flow at both the smoke-wire location and leading edge of the model. The stream velocity was approximately 4 m/s, and the wire was located 5 mm above the surface, or at roughly one-half the undisturbed boundary-layer thickness. The excitation voltage was 3 kV rms for Fig. 6a and 5 kV rms for Fig. 6b. Again, the plasma is not visible because of the intense photographic lighting. A notable feature of Figs. 6a and 6b is the convergence of the titanium dioxide streak lines toward the energized electrodes and the subsequent vortical mixing of the flow immediately downstream of the convergence region. This behavior is consistent with the attractive paraelectric body force observed in Fig. 5. What appears to be taking place is the formation of unstable, streamwise vortices driven by the paraelectric effects. Because of the higher electric fields in Fig. 6b than in Fig. 6a, the vortical structures develop sooner, are more compact, and break down sooner. In all the presence of the plasma generated by the symmetric electrode configuration constitutes a very strong boundary-layer tripping mechanism. The boundary-layer was also tripped in the case of spanwise electrodes (e.g., model C7-C), apparently because of the highly inflected streamwise velocity profiles, produced between the electrodes by the paraelectric forcing.[10]

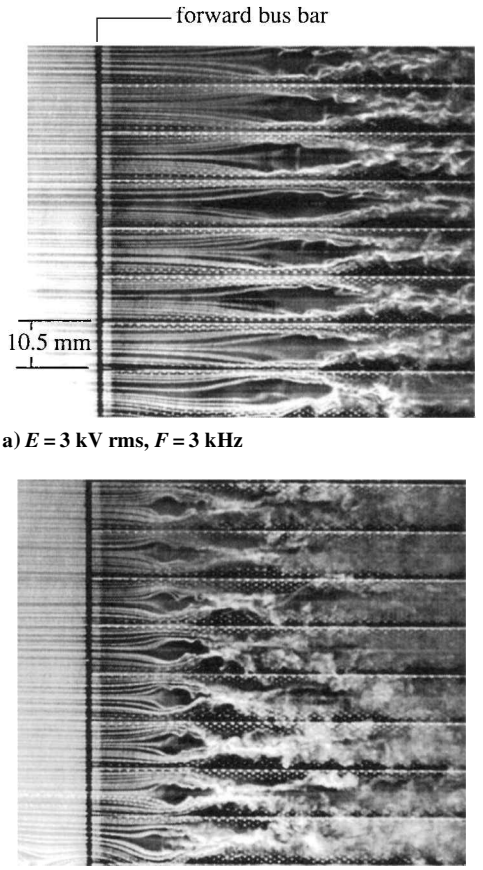


**a) $E$ = 3 kV rms, $F$ = 3 kHz**

**b) $E$ = 5 kV rms, $F$ = 3 kHz**

**Fig. 6 Smoke-wire flow visualization of panel C7-A: $U_\infty$ = 4 m/s.**

## Drag and Velocity Measurements

Drag and velocity profile data were acquired for all models listed in Table 1 for both energized (i.e., with plasma) and unenergized cases. Data were measured for flow velocities up to 26 m/s, electrode voltages up to 5.4 kV rms, and RF frequencies from 500 to 8000 Hz. The very small differences in surface roughness among different unenergized panels did not appear to measurably affect their drag. The roughness heights introduced by the copper electrodes are below the generally accepted limit for hydraulic smoothness of five viscous wall units, and therefore are not considered an important parameter in these studies. This is especially true when compared to the very large changes in drag and boundary-layer velocity profiles observed for the energized panels. Data were taken for both laminar and turbulent boundary-layer flow corresponding to the state of the flow at the leading edge of the unenergized model. Because the boundary layer was tripped with a small two-dimensional rod upstream of the panel, there was actually no case of completely undisturbed laminar flow in the sense of a Blasius profile. At low tunnel velocities, however, diagnostic hot-wire signals were devoid of any signs of turbulent breakdown.

Representative drag results from symmetric-planar electrode panels are shown in Fig. 7 for the streamwise electrode orientation (panel C7-A) and for the spanwise electrode orientation (panel C7-C). The drag coeffcient is equal to the ratio of the directly measured total drag of a model per unit model surface area to the freestream dynamic pressure. The unit Reynolds number is based on the freestream velocity and kinematic viscosity. Note the change in slope of the curves for the unenergized cases near $Re = 4 \times 10^5$/m, corresponding to transition from laminar to turbulent flow. For model C7-A with the plasma on, a substantial increase in drag is observed, which is caused by several factors. For laminar flow the plasma trips the flow to full turbulence, partially explaining the drag increase in that region. The drag increase persists, however, to the highest attainable velocity of the wind tunnel indicating that more than just flow tripping is involved. For model C7-C with plasma on, a smaller drag increase is produced and only in the

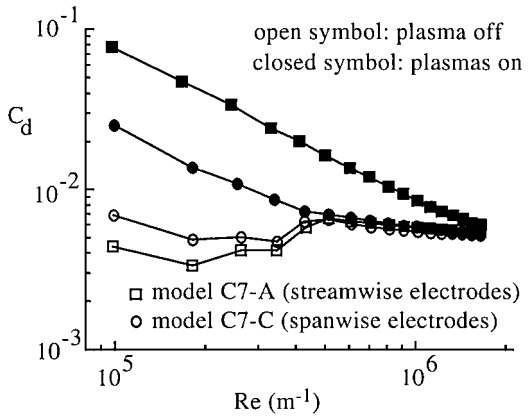


**Fig. 7 Effect of plasma and electrode orientation on directly measured drag: $E = 4$ kV rms and $F = 3$ kHz.**

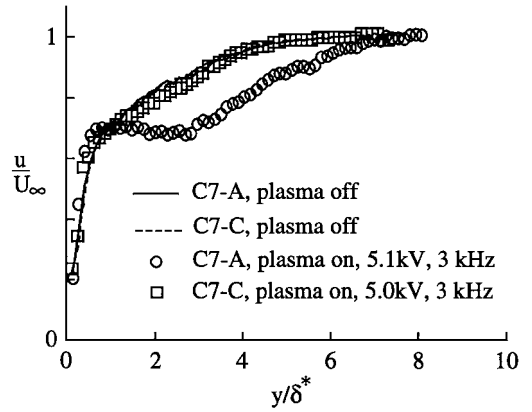


**Fig. 8 Effect of plasma and electrode orientation on boundary-layer velocity profiles.**

laminar/transitional region ($1 \times 10^5 < Re < 5 \times 10^5$/m). The difference in behavior between the two cases is consistent with the formation of plasma-driven, streamwise vortical structures in the boundary layer for the streamwise-oriented electrode configuration, consistent with the smoke-wire flow visualizations of Figs. 6a and 6b.

An important experimental drag error source was discovered early in the study. The observation was made that each of the plasma panels was acted on by an electrostatic force that was unrelated to the flow velocity leading to an error in measured drag. This force is induced by electric field lines, which originate on the panels and terminate on the grounded surroundings, with or without flow or plasma. It arises from the electrodynamic stress tensor. The electric field lines can be visualized as acting like rubber bands in tension between the panel electrodes and the grounded surroundings, producing an electrostatic pressure and a rms average force on the panel. The measured drag due to the electrostatic force was observed to vary quadratically with the applied rms excitation voltage. This is consistent with the known proportionality between electrostatic pressure and the square of the rms electric field. A force of up to 0.01 N was observed at 5 kV[6]. By replacing most metallic surfaces near the panel and drag balance with nonmetallic substitutes, the magnitude of the electrostatic force was reduced to insignificant levels. All drag data presented in this paper are either free from the electrostatic force effect or were corrected when it was above the resolution of our drag measurements (about 10 mg).

Boundary-layer velocity profiles were measured for several panels with symmetric and asymmetric electrode configurations. A total pressure probe was located about 28 mm, or approximately one undisturbed boundary-layer thickness downstream of the plasma. The probe tip was located over the smooth, aft filler plate of the lower wall. Figure 8 presents streamwise velocity profiles for models C7-A (streamwise electrodes) and C7-C (spanwise electrodes) at a unit Reynolds number of approximately $4.6 \times 10^5$/m, roughly the beginning of fully turbulent flow for the unenergized models in Fig. 7. For model C7-A the probe was positioned downstream and halfway between two adjacent electrodes. For model C7-C the probe was positioned downstream of the last electrode. A metallic aft plate was used for the profile measurements to allow use of a precise, solid-state electrical fouling indicator to aid measurement of the initial probe height location. As indicated earlier, for drag measurements a nonmetallic plate was used to minimize electrostatic drag error.

The profiles for the streamwise case (C7-A) show a large velocity deficit increase caused by the plasma. For the spanwise case in (C7-C) there is little difference between the energized and unenergized cases. These profiles corroborate the findings of the drag and smoke-wire investigations. For the streamwise electrode case the substantial increase in velocity deficit qualitatively corresponds to the large drag increase observed in Fig. 7. For the spanwise electrode configuration there is little effect on the drag at this unit Reynolds number. For the smoke-wire flow visualization, eruption of the vortical structures observed in Figs. 6a and 6b appear to be consistent with the flow retardation observed in the velocity profiles of Fig. 8. Additional data (not shown) indicate that data obtained downstream and directly behind a streamwise electrode were similar in both magnitude and shape to Fig. 8 for the energized and unenergized cases. Indeed, smoke-wire (e.g., Figs. 6a and 6b) and hot-wire diagnostics show that the energized, streamwise electrode patterns effectively trip the flow and that any between-electrode vs behind-electrode differences are largely mixed out by the end of the panel. The velocity deficit increase for the streamwise case was also significantly reduced at the highest tunnel velocity consistent with the merging of the energized and unenergized curves at $Re = 1.7 \times 10^6$/m in Fig. 7.

A final observation applicable to all energized OAUGDP flat panels relates to their acoustic behavior. Each panel produced a strong audible tone at the RF excitation frequency. The tone was present in unconfined, bench-top testing of the panels as well as in the enclosed wind-tunnel test section, ruling out any resonant chamber effects being responsible for the tone. It was initially suspected that the OAUGDP might be exciting a panel structural resonance. However, rigid mounting of the panel to its base plate did not appreciably change the pitch or intensity of the tone. The emitted sound therefore must be considered a direct coupling of the OAUGD plasma formation mechanism into radiated acoustic energy, a further indication of strong plasma-neutral gas coupling.

Probably the most interesting data taken during this study were those from the asymmetric panels, which were designed to unidirectionally accelerate the flow. The flow visualization of Figs. 6a and 6b with symmetric electrodes indicates an attraction of the flow toward the electrodes. If the electrodes are fabricated in an asymmetric staggered manner, such as the geometry illustrated in Fig. 1b., an unbalanced paraelectric EHD body force is exerted on the flow, and an equal and opposite reaction force is exerted on the panel on which the electrodes are mounted. The resultant force can be in the direction of the airflow (coflow), or opposite the freestream flow (counterflow) depending on the orientation of the electrode asymmetry. Figure 9 illustrates this force (thrust in this case) produced by panel E6-C mounted on the wind-tunnel drag balance without tunnel flow, plotted with respect to electrode voltage. Because of

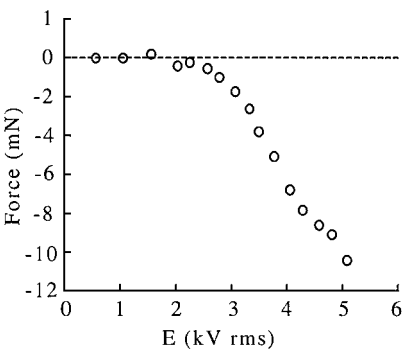


**Fig. 9 Thrust on model E6-C caused by asymmetric electrode design.**

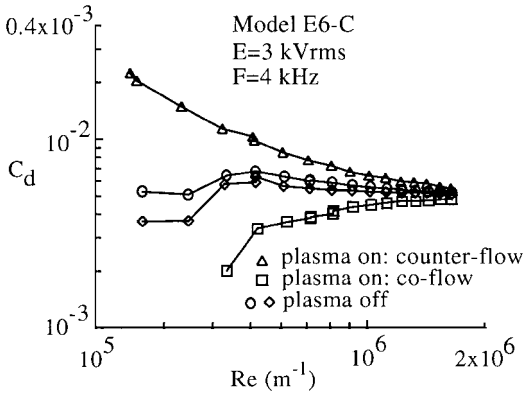


**Fig. 10 Effect of plasma and asymmetry direction on directly measured drag of model E6-C. (Coflow corresponds to lower electrode downstream of upper electrode.)**

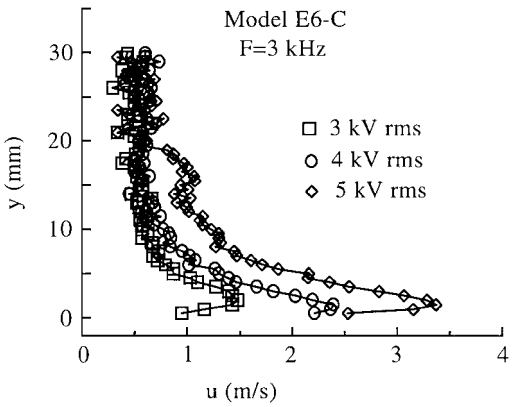


**Fig. 11 OAUGDP-induced velocity on model E6-C in still air: $F$ = 3 kHz.**

already mentioned wind-tunnel modifications, the electrostatic drag correction is insignificant. The plasma was operated at 3.0 kHz. The bottom electrodes were 3.0 mm wide and separated streamwise from the top electrodes by about 0.25 mm. The bottom electrodes were located downstream of the upper electrodes. As shown, for voltages less than about 1.5 kV, the approximate plasma initiation voltage, there is no force, proof that the force is caused by the plasma and paraelectric effects.

Figure 10 presents the drag on panel E6-C (the same model used in Fig. 9) over the usual tunnel velocity range. The plasma was operated at 4 kHz and 3 kV rms. The two curves corresponding to the unenergized cases approximately represent the smooth flat-plate reference drag data. The bottommost curve (plasma on: coflow) shows a reduction in drag comparable to the plasma-generated thrust. The upper-most curve (plasma on: counterflow) was taken with the same panel rotated 180 deg to generate a plasma-induced drag on the plate. Panel E6-C was not optimized for the paraelectric EHD force. While the predominant plasma forms on the upper surface on the edge corresponding to the nearest lower surface electrode (see Fig. 1b), a small amount of plasma forms on the opposite edge. The net effect is to have a large EHD force in one direction (downstream in the coflow case) and a smaller force in the opposite direction.

As a final diagnostic, the asymmetric panel E6-C was mounted in the wind tunnel with the flow off and with a pitot tube positioned at the same location used in Fig. 8. The resulting profiles of OAUGDP-induced velocity in the streamwise direction are shown in Fig. 11 for electrode voltages of 3, 4, and 5 kV rms. Maximum plasma-induced velocities up to 3.4 m/s were observed. A highly significant feature of these data is that the peak blowing velocity is linearly related to the applied voltage. This indicates that between the plasma initiation voltage and the limiting breakdown voltage of the gas at a given pressure (i.e., the glow-to-arc transition) a monotonically controllable effect is possible. (The reason for the 0.5 m/s offset at all voltages has not been investigated. Possible explanations include both instrumentation electromagnetic pickup errors caused by the high RF voltages and actual air entrainment caused by the plasma-induced wall jet.)

## Experimental Uncertainty

The purpose of this investigation was to provide a survey of the effects of the OAUGD plasma on airflow. The emphasis was on discerning basic physical phenomena using a broad range of complementary diagnostic techniques including direct drag, boundary-layer velocity profiles, and flow visualization. For this purpose an average quality accuracy consistent with good laboratory practice was judged to be acceptable. In general, data for individual readings of voltage, frequency, and displacement were estimated to be ±1% or better, flow velocities ±5%, unit Reynolds numbers ±10%, and drag coefficients ±15%.

## Discussion

The main finding of this investigation was the demonstration of a paraelectric flow-forcing mechanism associated with the OAUGD plasma. For the particular geometries tested, direct peak blowing velocities up to approximately 4 m/s were observed with proportionally large effects on directly measured drag and boundary-layer velocity profiles. Although the underlying physics of the OAUGDP is by itself reasonably well understood,[1,5] the paraelectric forcing mechanism requires additional study. In simple terms the forcing originates from the effect of nonuniformities in the local electric fields on the local net charge density in accordance with Poisson's equation [Eq. (2)]. A more detailed theoretical model of the strip electrode would involve solution of the coupled Maxwell and Navier–Stokes equations including provisions for the plasma chemistry, a potentially formidable task. Alternatively, one could effectively bracket the magnitude of the paraelectric body force by empirical observations over electric field strengths from plasma initiation to, say, glow-to-arc transition for a selection of electrode geometries. Based on the preliminary observations of this report, it appears unlikely that an order-of-magnitude increase in blowing velocity (from a single electrode pair) could be obtained. The paraelectric mechanism therefore appears to be a low-Reynolds-number phenomenon.

A more effective flow acceleration method would be to generate a peristaltic or traveling electric field along an array of multiple, spanwise-oriented strip electrodes.[4] In such a model each electrode would receive an excitation voltage slightly advanced in phase from its upstream neighbor. The result is a global, piecewise-continuous dc electric field that could be used to force the local charge distribution into motion and, via collisions, the neutral gas. The characteristic velocity in this case becomes the spatial phase velocity of the traveling electric field, which can be made arbitrarily high, until viscous effects become dominant. Clearly significant details need to be worked out, particularly with regard to the phasing between the net charge creation and the traveling wave. Traveling-wave acceleration, however, at least theoretically, circumvents the limitations of the paraelectric forcing method.

A final point of discussion involves the magnitude and role of local plasma heating. The question is whether any or all of the observed OAUGDP effects can be attributed to local density gradients. In general, it is difficult to construct a model to support a heating mechanism. In the case of the jet deflection in Fig. 5, for example, a buoyancy plume originating in the plasma would flow in the opposite direction. The experimental equipment required to measure the plasma temperature was not available for these tests, but there were several coarse, indirect temperature indicators. One is the fact that the plasma panels were fabricated from a plastic material with no more than several hundred degrees Celsius service capability. That fact that no melting occured is an indication of low plasma temperatures. The second indicator was cursory thermocouple readings in the boundary layer several inches downstream of an energized model. Temperatures of one or two degrees Celsius above ambient were noted, again consistent with a low plasma temperature.

Using 200°C as an estimate of the maximum plasma temperature based on the preceding indicators, a Grashof number can be computed. The Grashof number is a nondimensional indicator of

the magnitude of buoyancy forces relative to viscous forces and is given by[11]

$$Gr = [(gL^3/\nu^2)(\Delta T/T)] \quad (5)$$

Taking the characteristic dimension $L$ as the plasma-layer thickness, approximately 2 mm, $\Delta T$ as 200°C, $T$ the room ambient temperature of 293°K, and $\nu$ evaluated at ambient conditions, the Grashof number is approximately 230. Gebhart et al.[11] shows that the Reynolds number of a buoyancy-induced flow can be represented as the square root of the Grashof number. For the current case this would yield a value of approximately 15. For such a low thermally induced Reynolds number it is doubtful that buoyancy played a significant role in the phenomena observed during these experiments.

## Conclusions

Aerodynamic data have been acquired for planar models covered with strips of a uniform glow-discharge surface plasma at atmospheric pressure. Models with streamwise or spanwise arrays of flush, closely spaced, symmetric, or asymmetric plasma-generating surface electrodes were studied with laminar and fully turbulent boundary-layer flow in a low-speed wind tunnel. The observation was made that EHD forces can produce dramatic effects, which arise from paraelectric, RF forcing of the flow. Notable effects include large increases in measured drag caused by either vortex formation (symmetric electrode case) or directed thrust (asymmetric electrode case). In the more dramatic cases either flow acceleration or retardation affected the entire thickness of the boundary layer. The effects of heating are discounted, and the primary cause of the observed flow phenomena attributed to EHD forcing of the flow by a paraelectric RF body force.

## Acknowledgments

This research was a collaborative study by the University of Tennessee, Knoxville, and NASA Langley Research Center conducted under the auspices of the Chief Scientist (D. M. Bushnell), NASA Langley Research Center, Director's Discretionary Fund. The work of the first and second author was supported under NASA Langley Cooperative Agreement NCC-1-223.

## References

[1]Roth, J. R., *Industrial Plasma Engineering, Volume 1—Principles*, Inst. of Physics Publishing, Bristol, England, U.K., 1995.

[2]Roth, J. R., Tsai, P. P., and Liu, C., "Steady-State, Glow Discharge Plasma," U.S. Patent # 5,387,842, Feb. 1995.

[3]Roth, J. R., Tsai, P. P., Liu, C., Laroussi, M., and Spence, P. D., "One Atmosphere, Uniform Glow Discharge Plasma," U.S. Patent #5,414,324, May 1995.

[4]Roth, J. R., "Method and Apparatus for Covering Bodies with a Uniform Glow Discharge Plasma and Applications Thereof," U.S. Patent #5,669,583, Sept. 1997.

[5]Massines, F., Ben Gadri, R., Rabehi, A., Decomps, Ph., Segur, P., and Mayoux, Ch., "Experimental and Theoretical Study of a Glow Discharge at Atmospheric Pressure Controlled by Dielectric Barrier," *Journal of Applied Physics*, Vol. 83, No. 6, 1998, pp. 2950–2957.

[6]Roth, J. R., Sherman, D. M., and Wilkinson, S. P., "Boundary Layer Flow Control with a One Atmosphere Uniform Glow Discharge Plasma," AIAA Paper 98-0328, Jan. 1998.

[7]Malik, M. R., Weinstein, L. M., and Hussani, M. Y., "Ion Wind Drag Reduction," AIAA Paper 83-0231, Jan. 1983.

[8]El-Khabiry, S., and Colver, G. M., "Drag Reduction by DC Corona Discharge Along an Electrically Conductive Flat Plate for Small Reynolds Number Flow," *Physics of Fluids*, Vol. 9, No. 3, 1997, pp. 587–599.

[9]Pohl, H. A., *Dielectrophoresis, The Behavior of Neutral Matter in Nonuniform Electric Fields*, Cambridge Univ. Press, Cambridge, England, U.K., 1978, pp. 6–18.

[10]Sherman, D. M., "Manipulating Aerodynamic Boundary Layers Using an Electrohydrodynamic Effect Generated by a One Atmosphere Uniform Glow Discharge Plasma," M.S. Thesis, Dept. of Physics, Univ. of Tennessee, Knoxville, TN, Aug. 1998.

[11]Gebhart, B., Jaluria, Y., Mahajan, R. L., and Sammakia, B., *Buoyancy-Induced Flows and Transport*, Hemisphere, New York, 1988, pp. 9, 10.

P. Givi
*Associate Editor*